Nonlocal electrodynamics of arrays of quantum dots

Loys Belleguie and Shaul Mukamel
Department of Chemistry, University of Rochester, Rochester, New York 14627
(Received 6 September 1994; revised manuscript received 7 March 1995)

We analyze the linear and nonlinear optical responses of an array of quantum dots (QD's). Our model treats the matter-field interaction self-consistently, and includes the nonlocality of the electromagnetic field throughout the system. This procedure allows us to address the dependence of radiative decay rates as well as of the nonlinear response on size, geometry, and the material. Applications are made to a one-dimensional periodic array of semiconductor quantum dots, where the intradot and interdot exciton motion is of Wannier and Frenkel types, respectively. We compare the optical nonlinearity enhancement of the array with that of a single QD.

I. INTRODUCTION

Linear and nonlinear optical properties of semiconductor nanostructures, such as microcrystallites [spherical quantum dots (QD)], have been the subject of intense investigations in the last decade (see Ref. 1 and references therein). Theoretical studies have usually focused on the response of an isolated QD, treating the physical system (e.g., doped glasses) as an incoherent superposition of such microcrystals. Random assemblies of small particles have been studied for a long time, but periodic structures were fabricated only recently.[2] Studies have been conducted in an attempt to explore the effects of cooperativity arising when a periodic assembly of dielectric,[3,4] semiconductor,[5] or metallic particles of mesoscopic size interacts with an electromagnetic radiation (either microwave or optical). Dielectric spheres show Mie resonances in the microwave region. Yablonovich[3] has stressed the analogy between the electronic band structure of an atomic crystal and the photonic band structure of a crystal of dielectric spheres. Strong effects of cooperativity (i.e., coherent interference) are expected[5] for one-, two-, or three-dimensional arrays of semiconductor spheres, when the lattice constant is comparable to the optical wavelength.

We have calculated recently the optical response of a single semiconductor quantum dot (Ref. 6) in the weak confinement regime (exciton Bohr radius a_0 much smaller than the QD radius R), using a polariton picture. In this paper, we generalize this study and investigate the resonant linear and nonlinear properties of an array of semiconductor microcrystallites. The optical response of each QD is described by a Wannier exciton model, and shows a series of quantized exciton levels with radiative widths. The interdot dynamics of an assembly of such QD's is conveniently expressed in a Frenkel-exciton model.[7–9] The present study combines several well established concepts, such as the quasiatomic optical properties of a QD and the Frenkel-exciton description of a macroscopic coherent excitation in an assembly, of QD's. In an artificial assembly, we can vary the intrinsic parameters such as the material size, the geometry, lattice constant, and the symmetry of the array. Various properties such as radiative lifetime or nonradiative damping arising from phonon coupling can be controlled as well.

Excitons in molecular crystals can usually be described adequately using a two-level model for the material, with dipole-dipole intermolecular interaction. These are justified since the exciton bandwidth is typically two orders of magnitude smaller than the atomic (or molecular) electronic frequencies. These assumptions may not hold for quantum dot arrays, particularly when R increases and $R/a \to 1/2$ (close packing), where a is the lattice parameter. Under these conditions, the spacing between quantized states becomes comparable to the Frenkel-exciton bandwidth. For example, in the mesoscopic region (starting around $10a_0$, a_0 being the bulk-exciton Bohr radius), both are of the order of a fraction of the bulk-exciton binding energy. Taking CuCl, the energy difference between the lowest radiative exciton states is $\Delta_c = \varepsilon_2 - \varepsilon_1$ of the order of 10 meV for $R = 10a_0$, and $\Delta_c \simeq 0.75$ meV for $R = 40a_0$, and the interdot interaction Δ_{dip} of the order of 1 meV for both sizes. We can, therefore, no longer treat the QD's as two-level molecules and we must find the eigenmodes of the system directly from the interacting multilevel QD system. The assembly is then better treated using a band-structure calculation, such as the KKR method.[10] Our formalism is rather general and describes the excitations of semiconductor quantum dots of arbitrary size as Wannier excitons. Frenkel-exciton polaritons are found when the QD size is small enough, and analytical results can be derived in this case.

In this paper, we consider arrays of ideal quantum dots made of a semiconductor. We assume infinite confining potential wells on the surface of each QD. Therefore, electronic wave functions do not overlap between different dots. Intradot excitonic motion is then of Wannier type and confined in one QD, whereas interdot propagation is described as a Frenkel excitation. Nonlinearities on the other hand arise only from the overlap of excitonic wave functions, as well as Coulomb interaction inside one quantum dot. We do not include the possibility of decoupling of electron and hole motion between different dots. As a consequence, we can generalize to the array the

derivation presented in a recent paper[6] for a single QD.

Takagahara[11] has pointed out that the Frenkel exciton created in the array can induce large nonlinearities since its effective mass, which is inversely proportional to the transfer energy between QD, can be much smaller than that of excitons in molecular crystals. The third-order nonlinearity at the Frenkel-exciton resonance is inversely proportional to the effective mass. The density of states is proportional to the effective mass, and it must be small in order to maintain a large coherence length and oscillator strength. However, this simple argument is not rigorous, because of the strength of nonlocal effects in the interaction between QD's. First, the band structure is affected by the interplay of higher states with $l > 0$ (see below). In the Frenkel exciton limit, one can isolate one s-exciton state in each sphere and calculate the response of an assembly of two-level molecules. This limit corresponds to the point-dipole approximation and will serve as a reference for all the calculations made in this paper. Following Ref. 11, we shall study the possible coherent enhancement of the nonlinearities and its limitations. The oscillator strength is proportional to the QD volume, as long as $R/a_0 \gg 1$. As has been shown in Ref. 6, the enhancement of each QD is limited. The mixing of QD's Frenkel states will give rise to a saturation of the oscillator strength by scattering on many possible channels. Therefore, the optimal set of parameters (R, a, exciton dipole moment μ_{cv}, and nonradiative damping γ_{nr}) which yield the largest enhancement will depend crucially on nonlocal effects. Hereafter, μ_{cv} denotes the dipole moment between conduction and valence bands.

In Sec. II, we present the model and the method for calculating the linear optical response of an array of quantum dots. We then apply the theory to the case of large semiconductor QD's in Secs. III and to small QD's in Sec. IV. Nonlinear response is discussed in Sec. V, and a more general procedure, which calculates the field directly and addresses the problem of photonic band structure, using the same formalism is presented in Sec. VI.

II. LINEAR OPTICAL RESPONSE OF A SEMICONDUCTOR QD ARRAY NEAR EXCITON RESONANCES

We consider an array of semiconductor quantum dots. The array can be of any dimensionality, and is characterized by its size, the number of QD's in each dimension, and the lattice symmetry. We focus on exciton transitions in the vicinity of the band gap. Each QD is characterized by its own excitonic level scheme and dipole moment. For simplicity, we assume an infinite confining potential at the surface of each QD. Therefore, electron-hole excitation are confined in the same dot. As a consequence, no overlap exists between electronic wave functions belonging to different sites.

The excitation is described by a delocalized exciton interacting with the light field, forming a polariton. Since we are primarily interested in the properties of the material system (resonances of the QD), we shall focus on the polarization instead of the field, following a procedure outlined in Ref. 6. The polarization and the field are directly related, and we are free to choose one of these quantities as our primary variable.

From the assumptions introduced just above, the Hamiltonian is similar in every respect to that of a single QD, except that the confining potential becomes[6]

$$V_{\rm conf}(\vec{r}) = \sum_{\vec{R}_n} V^0_{\rm conf}(\vec{r} - \vec{R}_n), \tag{1}$$

where

$$V^0_{\rm conf}(\vec{r} - \vec{R}_n) = 0 \text{ for } r < R \text{ and } \infty \text{ for } r \geq R \tag{2}$$

is the potential of one QD. Therefore, we can start from the Fourier transform of equation (16) in Ref. 6, where the exciton envelope $P^{(1)}_{12}(\vec{r}_e, \vec{r}_h)$ [denoted $\psi(\vec{r}_e, \vec{r}_h)$ here] represents the expectation value of the annihilation operator for an electron-hole pair $\Psi_e(\vec{r}_e)\Psi_h(\vec{r}_h)$, $\vec{r}_e$, and $\vec{r}_h$ being the electron and hole coordinates, respectively. The optical polarization is then given by

$$P(\vec{r}) = \hat{\mu}_{\rm cv}\left[\psi(\vec{r},\vec{r}) + \psi(\vec{r},\vec{r})^*\right], \tag{3}$$

where $\hat{\mu}_{\rm cv}$ is the band-to-band exciton dipole moment. The linearized effective exciton equation of motion for the array is

$$\left(-i\hbar\frac{\partial}{\partial t} + H_c\right)\psi(\vec{r}_e,\vec{r}_h;t) - \delta(\vec{r}_e - \vec{r}_h)\sum_n \int_\Omega d\vec{x}' \int_{-\infty}^{t} dt' \times \Sigma(\vec{r}_e,\vec{r}';t-t')\psi(\vec{r}',\vec{r}';t')\delta(\vec{r}' - \vec{x}' - \vec{R}_n) = \delta(\vec{r}_e - \vec{r}_h)\hat{\mu}_{\rm cv}\cdot\vec{E}_0(\vec{r}_e,t), \tag{4}$$

where $\vec{R}_n$ are the positions of the QD's, Ω their volume, and $\vec{E}_0(\vec{r})$ is the external applied field. Hereafter integrals over $\vec{r}$ apply to the whole system, whereas integrals on $\vec{x}$ refer to the volume of one quantum dot. H_c contains the kinetic and direct Coulomb interaction operators. Equation (4) is a generalization of Eq. (20) of Ref. 6. Note, however, that some misprints survive in this last reference. Equations (4) and (5) constitute the proper definitions. The self energy Σ contains all the relevant information on the array (scattering on other QD's and radiative decay rates in each QD), and is given by

$$\Sigma(\vec{r},\vec{r}';t) = \int \frac{d\omega}{2\pi}\,\Sigma(\vec{r},\vec{r}';\omega)e^{-i\omega t}, \tag{5}$$

$$\Sigma(\vec{r},\vec{r}';\omega) = \hat{\mu}_{\rm cv}\cdot\left\{\frac{\omega^2}{c^2} + \vec{\nabla}\vec{\nabla}\cdot\right\}\frac{e^{i\frac{\omega}{c}|\vec{r}-\vec{r}'|}}{|\vec{r}-\vec{r}'|}\hat{\mu}_{\rm cv}.$$

This equation defines the macroscopic exciton states as the lowest excited states of the array. Equation (4) holds for all confinement regimes. In particular, it can be applied for strong confinement when the direct electron hole Coulomb interaction is negligeable compared to the kinetic energy. This regime applies usually for particles much smaller than the wavelength (e.g., CdS or CdSe

quantum dots with radii of the order of few nanometers[2]). In this case, one can neglect the spatial dependence of the wave function inside the QD's (in the integral in 4), and Eq. (4) reduces to a lattice sum, as in the point-dipole approximation. However, this approximation is less justified here than in molecular crystals. By expanding the exciton wave function in single QD wave functions, integrals like in (4) are easily evaluated. In the opposite, weak confinement limit, where the exciton Bohr radius is much smaller than the QD size, this size can be comparable to the wavelength. In mesoscopic QD arrays the ratio of array lattice constant to the wavelength can approach unity.

Let us first consider a finite assembly of N identical QD's. The exciton amplitude $\psi(\vec{r}_e,\vec{r}_h)$ is expanded as a linear combination of the eigenfunctions $\phi_a(\vec{r}_e,\vec{r}_h)$ of the single-QD Hamiltonian H_c. Since our model assumes that no overlap can exist between the QD's, no decoupling of the electron-hole relative motion in different dots can arise. Therefore, the wave function can be written

$$\psi(\vec{r}_e,\vec{r}_h)=\sum_{n,a} C_{n,a}\ \phi_a(\vec{r}_e-\vec{R}_n,\vec{r}_h-\vec{R}_n). \tag{6}$$

This form of the wave function then implies that the excitation is of Wannier type inside the QD and propagates as a Frenkel exciton throughout the array.

The Fourier transform of the linear exciton Green function [Green function of Eq. (4)] can be written in real space as

$$G^{\rm exc}_{na,n'a'}(\omega)=\left\langle n,a\left|\frac{1}{\hbar\omega-H_{\rm eff}(\omega)}\right|n',a'\right\rangle, \tag{7}$$

where

$$H_{\rm eff}(\omega)=H_c-\Sigma(\omega). \tag{8}$$

$H_{\rm eff}$ is the nonlocal (in time and space) effective Hamiltonian containing the self-energy, due to the electromagnetic field degrees of freedom. The set of quantum numbers $\{n,a\}$ corresponds to the sites and Wannier exciton levels on each site. The matrix elements of Σ are given in this basis by

$$\Sigma_{n'a',na}(\omega)=\int d\vec{r}\int d\vec{r}\,'\phi^*_{a'}(\vec{r}-\vec{R}_{n'},\vec{r}-\vec{R}_{n'})\times\Sigma(\vec{r},\vec{r}\,';\omega)\phi_a(\vec{r}\,'-\vec{R}_n,\vec{r}\,'-\vec{R}_n). \tag{9}$$

If L states are considered in each QD, we can then calculate the optical response using a $NL\times NL$ matrix. The numerical effort of this procedure grows with system size, nevertheless it can be applied to rather large systems in the one-dimensional case.

Compared to the single-QD case, the interaction between different QD's brings new states (described, for example, by a Bloch wave vector $\vec{k}$ in the case of an infinite system), which have a strong cooperative character. If the QD size is sufficiently small, one can treat the interaction of the field with each QD in the long wavelength approximation. We then recover the Frenkel-exciton (molecular) limit.

We shall base our calculation of the linear and nonlinear optical properties of the QD array on the Green function (7). In the case of an infinite and periodic system (at least one infinite dimension), the one-exciton states are described by a Bloch wave vector $\vec{k}$ together with the indices of single-QD exciton states. Then, the delocalized exciton states will have the following eigenfunctions,

$$\psi_{\vec{k}}(\vec{r}_e,\vec{r}_h)=\sum_n e^{i\vec{k}\cdot\vec{R}_n}f_{\vec{k}}(\vec{r}_e,\vec{r}_h;\vec{R}_n), \tag{10}$$

$$f_{\vec{k}}(\vec{r}_e,\vec{r}_h;\vec{R}_n)=\sum_a C_a(\vec{k})\phi_a(\vec{r}_e-\vec{R}_n,\vec{r}_h-\vec{R}_n),$$

where the energies and the coefficients $C_a(\vec{k})$ are given by the eigenvalues and eigenvectors of the matrix,

$$(H_{\rm eff})_{aa'}(\omega,\vec{k})=(H_c)_a\delta_{aa'}-\Sigma_{aa'}(\omega,\vec{k}). \tag{11}$$

The self-energy $\Sigma_{aa'}(\omega,\vec{k})$ is calculated in Appendix A. Equation (11) contains all radiative corrections to the dipole-dipole interaction between spheres. Due to retardation, the excitation energies should be calculated from the poles of the resolvent matrix $G(z,\vec{k})=1/[z-H_{\rm eff}(z,\vec{k})]$. The poles and residues of this matrix are given to a good accuracy by the Markov (or pole) approximation, which neglects the energy dependence of the self-energy by writing $\Sigma(\omega)\simeq\Sigma(E_{\rm av})$ where $E_{\rm av}$ is an average of the nonperturbed eigenvalues of $(H_c)_a$. Denoting the resulting eigenvalues by $\varepsilon_\lambda(\vec{k})-i\gamma_\lambda(\vec{k})$, the retarded Green function may be written near resonance:

$$G(\vec{r},\vec{r}\,';\omega)=\sum_{\lambda\vec{k}}\frac{\psi_{\vec{k}\lambda}(\vec{r},\vec{r})^*\psi_{\vec{k}\lambda}(\vec{r}\,',\vec{r}\,')}{\hbar\omega-\varepsilon_\lambda(\vec{k})+i\gamma_\lambda(\vec{k})}, \tag{12}$$

and the linear polarization is given by

$$\vec{P}^{(1)}(\vec{r})=-\hat{\mu}_{\rm cv}\int d\vec{r}\,'\ G(\vec{r},\vec{r}\,';\omega)\hat{\mu}_{\rm cv}\cdot\vec{E}_0(\vec{r}\,'). \tag{13}$$

The numerical procedure employed below allows us, however, to calculate exactly the real poles and residues of the exciton Green function without invoking the pole approximation. In practice, we calculate the Green function matrix elements on a grid of $(\vec{k},\omega)$ values and using spline functions, we express these elements as continuous functions in $(\vec{k},\omega)$. The poles and residues are then located and evaluated numerically. The advantage of this procedure is that we obtain a function of $\vec{k}$ that can be used for calculating the third-order response (see Sec. V). Non-Markovian polariton effects can be incorporated as well, by keeping the resolvent matrix $G(\omega,\vec{k})$ in its original form [a different matrix for each $(\omega,\vec{k})$]. However, the diagonal approximation (12) is much simpler for calculating the nonlinear polarization which involves products and integrals of this resolvent. Non-Markovian effects mainly occur in a small region near $k=q$ ($q\equiv\omega/c$), where the mixing between exciton and photon is very strong.[8] We will disregard these effects here, since we want to investigate the nonlinear response near $k=0$. In concluding this section, we note that using the results

of Refs. 6, and 9, all linear and third-order nonlinear response functions of the array will be determined by the one-exciton Green function [Eq. (7) for a finite assembly or Eq. (12) for a periodic infinite array].

III. APPLICATION TO AN ARRAY OF WEAKLY CONFINED SEMICONDUCTOR QUANTUM DOTS

We consider an array of large, weakly confined, semiconductor quantum dots. We assume a nondegenerate two-band semiconductor in the effective-mass approximation and use the center of mass quantization approximation.[12] In Eq. (4), the operator H_c then becomes

$$H_c = \varepsilon_{\rm ex} - \frac{\hbar^2}{2M}\nabla^2_{\vec{r}}, \tag{14}$$

where M is the exciton mass and $\varepsilon_{\rm ex}$ the bulk-exciton energy. Only the electron-hole pair center of mass coordinate remains in the equation of motion, due to the factorization of the relative motion. The QD-exciton states are described by three quantum numbers $\{n\ell m\}$, $n = 1, 2, ...; \ell \geq 0; -\ell \leq m \leq \ell$.[12] Note that n and ℓ are independent and there exists an infinite number of levels characterized by n in each subspace defined by (ℓ, m) (with the spherical harmonics basis). n should not be confused with the principal quantum number in the hydrogen atom for which $\ell = 0, \ldots, n-1$.

We consider a one-dimensional chain along the $\hat{z}$ axis made of identical QD's with radius R and lattice constant a. We assume that the exciton-transition dipole moment is oriented in the (x, z) plane making an angle θ with $\hat{z}$.

The exciton dispersion curve $\varepsilon_\lambda(\vec{k})$ is plotted in Fig. 1 for two directions of the dipole moment. We assumed a close-packed linear chain, with QD radius $R = 40a_0$ and $a = 2R$. We use the Markov approximation, which is adequate for the poles of the exciton Green function. These results are similar to those of Ref. 8. We took only exciton states with $\ell \leq 2$ and $n \leq 5$. Exciton states with $l = 1$ play a negligible role here. They are actually not connected with $l = 0$ and $l = 2$ states in the case of a single sphere and give a small contribution for the array. Higher quantum numbers are more important when R increases so that the bandwidth becomes comparable with the spacing between exciton states.

Figures 1(a) and 1(b) show the real energies and radiative decay rates of the three strongest optically active exciton states for $\theta = (\hat{\mu}_{\rm cv}, \hat{z}) = 0$. Figures 1(c) and 1(d) correspond to $\theta = \pi/2$. Calculations are given in units of E_R, the exciton Rydberg (binding) energy in the bulk which is related to the exciton Bohr radius by the formula $e^{*2}/2a_0$, e^* being the effective electron charge in the material. Dashed lines were obtained by including only the $\ell = 0$ QD-exciton states. This corresponds to the point-dipole approximation, which is expected to hold in the case of very small QD's and, in particular, for molecular crystals. The present calculations show its limitations due to the increase in QD-exciton density of states. Delocalized optically active exciton states, therefore, have a strong p and d component. These curves have the characteristic exciton dispersion law in a one-dimensional crystal,[8] which shows a logarithmic divergence near the point $\omega = kc$. This divergence is, however, removed if one makes the full polariton calculation without the Markov approximation. The radiative exciton disappears when $kc > \omega$, due to energy conservation. It also shows the super-radiant concentration of oscillator strength (or radiative decay rate) on few levels. Contrary to the two-level system case with the point-dipole approximation, pure superradiance is lost due to mixing with states of lower symmetry ($\ell \neq 0$). This limitation of the super-radiant enhancement is related not to the chain size, but rather to the quantum-dot size.

In Appendix B, we derive a closed expression for the polariton dispersion when one neglects the $\ell \neq 0$ exciton states. We find that for an infinite array with arbitrary dimensionality ($d = 1, 2$ or 3), the s-exciton dispersion is determined by the following equation for ω ($q \equiv \omega/c$):

$$D(\vec{k}, \omega) = \frac{1}{C(q, \vec{k})} + \sum_n \frac{f_n(q)^2}{\hbar\omega - \varepsilon_n} = 0, \tag{15}$$

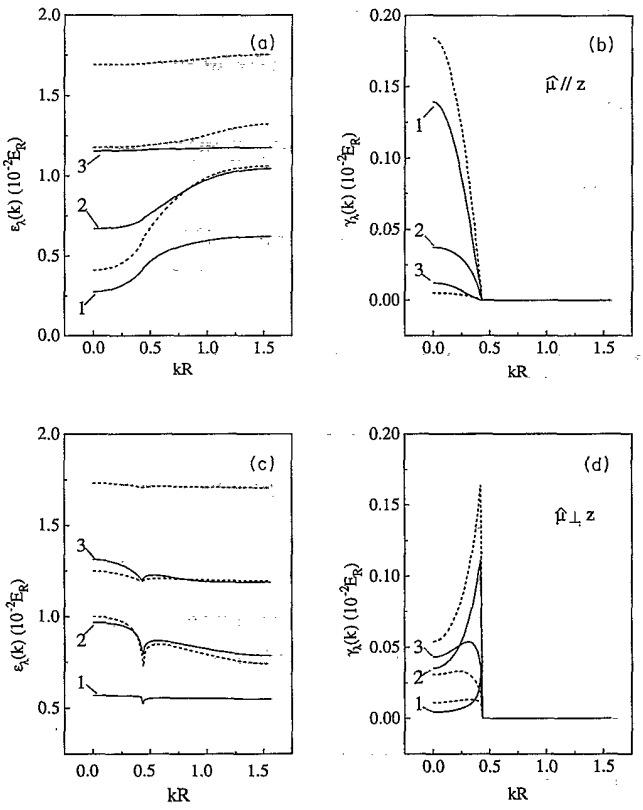

FIG. 1. Exciton-polariton dispersion curves for a linear chain of semiconductor QD's of radii $R = 40a_0$. The lattice constant is $a = 2R$. Panels (a) and (b) show the real energies and radiative decay rates of the polariton for $\theta = (\hat{\mu}_{\rm cv}, \hat{z}) = 0$, respectively. Panels (c) and (d) correspond to $\theta = \pi/2$. Dashed curves were calculated with only $\ell = 0$ exciton states. All quantities are given in units of E_R.

where $C(q,\vec{k})$ is complex, and all quantities appearing in this equation are defined in Appendix B. The cooperativity between QD's is determined by the factor $C(q,\vec{k})$, which is related to the structure factor.

From Eq. (15), we can rationalize the existence of super-radiant and subradiant macroscopic excitons. The exciton-polariton density of states (DOS) at a given $\vec{k}$ value can be calculated exactly from our model and is given by the imaginary part of the trace of the one-exciton Green function as

$$\rho(\vec{k},\omega) = -\,\mathrm{Im}\left\{\frac{1}{D(\vec{k},\omega)}\sum_{n\geq 1}\frac{1/C(q,\vec{k})+\sum_{i\neq n}\frac{f_i(q)^2}{\hbar\omega-\varepsilon_i}}{(\hbar\omega-\varepsilon_n)}\right\}. \tag{16}$$

This is displayed graphically in Fig. 2. For large sizes, the resonances are very close, and the residues of ρ [proportional to the inverse of the derivative of $\mathrm{Re}D(\omega)$] are large except for the first level [Fig. 2(a)]. This signature of super-radiant versus subradiant behavior explains the dashed curves in Figs. 1(b) and 1(d). On the other hand, when the QD's are sufficiently small, the resonant energies are well separated, and the residues are almost constant for each state [Fig. 2(b)]. They are only weighted by the single-QD oscillator strength f_n, showing that the macrocospic states are shared in the same way as in an isolated QD. The insets show the derivative of $\mathrm{Re}D(\omega)$, and the arrows indicate the location of the poles.

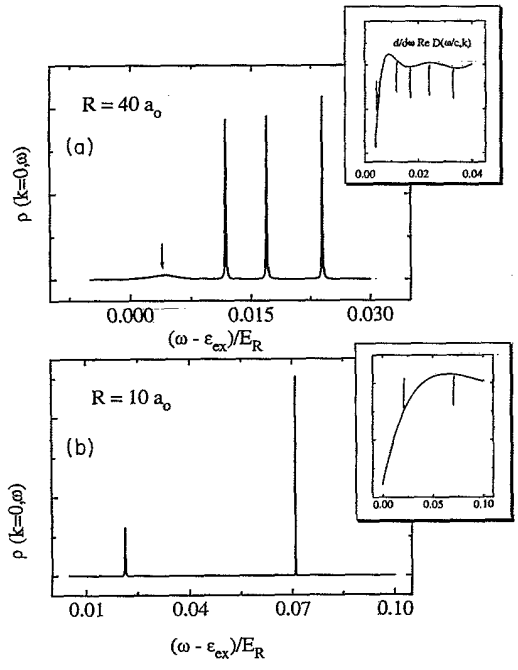

FIG. 2. One-dimensional exciton-polariton density of states given by Eq. (16). Panel (a) shows large radius and panel (b) correspond to smaller radius (see text).

IV. APPLICATION TO SMALL SEMICONDUCTOR QUANTUM DOTS (STRONG CONFINEMENT)

Small (few nanometer) semiconductor quantum dots of a large class of materials show strong confinement, since the exciton Bohr radius is larger than their size. This limit is particularly interesting because small QD's, whose sizes range from 1.5 nm to 5 nm in radius, may be grown in periodic arrays.[2]

Single-quantum-dot-exciton levels are widely spaced in the strong confinement limit, and we can focus on one level and treat the system using the Frenkel-exciton model. We assume the simplest form of the operator H_c in Eq. (4),

$$H_c = E_G - \frac{\hbar^2}{2m_e}\nabla^2_{\vec{r}_e} - \frac{\hbar^2}{2m_h}\nabla^2_{\vec{r}_h}, \tag{17}$$

where E_G is the energy gap and m_e, m_h the electron and hole effective masses. We neglect Coulomb interaction compared to the kinetic energy. The lowest exciton wave function is given by

$$\psi(\vec{r}_e,\vec{r}_h) = \frac{\pi}{2R^3}\, j_0(\pi r_e/R) j_0(\pi r_h/R)\ , \tag{18}$$

with energy

$$\varepsilon_{\mathrm{ex}} = E_G + \frac{\hbar^2}{2\mu R^2}\pi^2, \tag{19}$$

where j_0 are Bessel functions of zeroth order, and $1/\mu = 1/m_e + 1/m_h$ is the exciton reduced mass. This wave function is the first term of the representation of the exact wave function in Bessel functions[14] when the Coulomb interaction is added to H_c. It is a very good approximation for sufficiently small QD's. We concentrate here on the main features and important properties of the array.

Using the formalism of Sec. II and the results of Appendix C, and making the long wavelength approximation on each QD (but not on the lattice parameter length scale), we calculate the macroscopic exciton states of the array. The dipole-dipole and retarded interactions (self-energy Σ) are in this limit proportional to the ratio of exciton and QD volumes and are, therefore, enhanced compared with larger sizes (cf. Appendix C) for which the matrix Σ does not depend on the volume. The polariton dispersion relation is now given by the solutions of [cf. Eq. (B4)]

$$\hbar\omega = \varepsilon_{\mathrm{ex}} + \frac{\Delta_{\mathrm{LT}}}{(R/a_0)^3}\left[z_0(q) + C(q,\vec{k})\right], \tag{20}$$

where

$$z_0(q) \simeq (-0.45q^2 + 2.1\tilde{\mu}^2) + i(0.25 - 0.24\tilde{\mu}^2 q^3)\ ,$$

$$C(q,\vec{k}) \simeq i\frac{q^3}{4}J^{00}_{0000}(q,\vec{k}) - 0.028q^3\left(\sum_{Li} J^{1-i}_{L0,1-j}(q,\vec{k})\tilde{\mu}_i^2\right).$$

The function J is defined by Eq. (A6) and $\tilde{\mu}_i = \mu_{\mathrm{cv},i}(00|1-i1i)$. In Eq. (20), we apply the long wave-

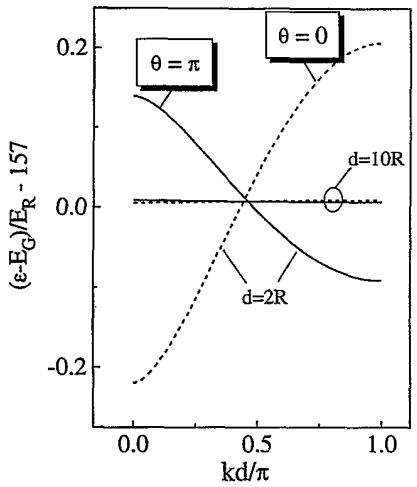

FIG. 3. Exciton-polariton dispersion curve for a one-dimensional array of GaAs QD's of radii $R = 0.25a_0$ with two different lattice constants $a = 2R$ and $a = 10R$. $\theta = (\hat{\mu}_{cv}, \hat{z}) = 0$ and $\theta = \pi$, respectively.

length approximation on the level of one quantum dot by keeping only the first term in the expansion of the intradot interaction matrix elements in q.

In Fig. 3, we show the dispersion curve of the macroscopic exciton of a one-dimensional array of small semiconductor QD's of radii $R = 0.25a_0$. The lattice constant is $a = 2R$, and $a = 10R$. Solid curves correpond to $\hat{\mu}_{cv} \perp \hat{z}$ and dashed curves to $\hat{\mu}_{cv} \parallel \hat{z}$. We used parameters of GaAs, where the bulk exciton radius is 140 Å.

V. TWO-PHOTON ABSORPTION OF AN ARRAY OF LARGE QD'S

Once the exciton Green function of the array is calculated, we can express the third-order polarization and the scattered field in terms of the external field. The linear polarization is[6]

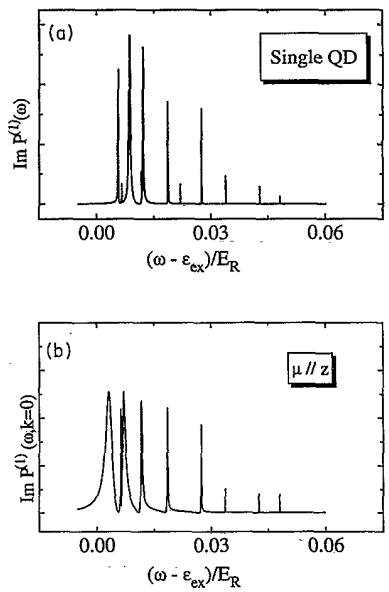

FIG. 4. The upper panel shows imaginary part of the linear polarization of a single weakly confined QD ($R = 40a_0$). The lower panel shows the case of a chain of weakly confined QD's. The lattice constant is $a = 2R$ and $\hat{\mu}_{cv} \parallel \hat{z} = 0$.

$$\vec{P}^{(1)}_{\nu_s}(\vec{k}_s, \omega_s) = -\hat{\mu}_{cv} \sum_{\nu'_s} G_{\nu_s \nu'_s}(\omega_s, \vec{k}_s) E_{0\nu'_s}(\omega_s, \vec{k}_s). \quad (21)$$

Figure 4 (lower panel) shows the imaginary part of the linear polarization of a linear chain of quantum dots with $R = 40a_0$ with a dipole moment parallel to the chain axis and for $k = 0$ excitons. The nonradiative damping is $\gamma_{nr} = 10^{-4}E_R$. The upper panel shows the linear polarization for a single quantum dot. We see that the cooperativity brought by the array makes the lowest Frenkel-exciton level more dominant. This is favorable for enhancing the nonlinearities.

The third-order polarization is given by[6]

$$\vec{P}^{(3)}_{\nu_s}(\vec{k}_s, \omega_s) = \hat{\mu}_{cv} \sum_{\nu_1\nu_2\nu_3} \chi^{(3),c}_{\nu_s\nu_1\nu_2\nu_3}(-\vec{k}_s, -\omega_s, \vec{k}_1, \omega_1, \vec{k}_2, \omega_2, \vec{k}_3, \omega_3) E_{0\nu_1}(\omega_1, \vec{k}_1) E_{0\nu_2}(\omega_2, \vec{k}_2) E_{0\nu_3}(\omega_3, \vec{k}_3)$$
$$+\hat{\mu}_{cv} \sum_{\nu_1\nu_3\nu'_s\nu'_1\nu'_3} \chi^{(3),p}_{\nu_1\nu_3\nu'_s\nu'_1\nu'_3}(-\vec{k}_s, -\omega_s, \vec{k}_1, \omega_1, \vec{k}_2, \omega_2, \vec{k}_3, \omega_3) E_{0\nu_1}(\omega_1, \vec{k}_1) E^x_{0\nu'_s\nu'_1\nu'_3}(\omega_2, \vec{k}_2) E_{0\nu_3}(\omega_3, \vec{k}_3), \quad (22)$$

where $\omega_s = \omega_1 + \omega_2 + \omega_3$ and $\vec{k}_s = \vec{k}_1 + \vec{k}_2 + \vec{k}_3$ and

$$\chi^{(3),c}_{\nu_s\nu_1\nu_2\nu_3} = \sum_{\nu'_s\nu'_1\nu'_2\nu'_3} G_{\nu_s\nu'_s}(\omega_s, \vec{k}_s) G_{\nu'_3\nu_3}(-\omega_3, -\vec{k}_3)^* \times \Gamma_{\nu'_s\nu'_3\nu'_1\nu'_2}(\omega_1 + \omega_2, \vec{k}_1 + \vec{k}_2) G_{\nu'_1\nu_1}(\omega_1, \vec{k}_1) \times G_{\nu'_2\nu_2}(\omega_2, \vec{k}_2), \quad (23)$$

$$\chi^{(3),p}_{\nu_1\nu_3\nu'_s\nu'_1\nu'_3} = G_{\nu_s\nu'_s}(\omega_s, \vec{k}_s) G_{\nu'_3\nu_3}(-\omega_3, -\vec{k}_3)^* \times G_{\nu'_1\nu_1}(\omega_1, \vec{k}_1). \quad (24)$$

The superscript c refers to the exciton-exciton Coulomb interaction contribution, whereas p refers to the Pauli exclusion contribution. We have further denoted

$$\Gamma(\omega, \vec{k}) = \frac{V}{1 - \frac{V}{2i\pi} \int d\vec{k}' \int d\omega' \; G(\omega', \vec{k}') G(\omega - \omega', \vec{k} - \vec{k}')}, \quad (25)$$

where V is the exciton-exciton interaction matrix, and

$$E_{0\nu}(\omega,\vec{k}) = \int_\Omega d\vec{r}\ \psi_\nu(\vec{r},\vec{r})\hat{\mu}_{\rm cv}\cdot\vec{E}_0(\vec{r},\omega,\vec{k}), \quad (26)$$

$$E^x_{0\nu_1\nu_2\nu_3}(\omega,\vec{k}) = \int_\Omega d\vec{r}d\vec{r}_e d\vec{r}_h\ \psi_{\nu_1}(\vec{r}_e,\vec{r}_h)^*\psi_{\nu_2}(\vec{r}_e,\vec{r}) \times\psi_{\nu_3}(\vec{r},\vec{r}_h)\hat{\mu}_{\rm cv}\cdot\vec{E}_0(\vec{r},\omega,\vec{k}). \quad (27)$$

The above expressions should be understood as matrices in the space defined by the eigenvalues of the unperturbed Hamiltonian H_c. Equation (22) is the Green function solution of the semiconductor Bloch equations[13,14] in the low density limit. Here, we keep the form obtained in Ref. 6, which can be applied to quantum dots of any size. Intermediate sizes, i.e., $R \sim a_0$, are the most demanding computationally, due to the number of exciton states involved.[1] However, useful simplifications can be made in the extreme strong or weak confinement limits. For instance, small GaAs quantum dots (e.g., $R \simeq 30$ Å$\sim 0.2a_0$) or large CuCl QD's (e.g., $R \simeq 140$ Å$\sim 20a_0$), where the center of mass approximation can be used.

For weak confinement, one can keep only the first exciton-exciton interaction term in the right-hand side of Eq. (22),[6] whereas in the strong confinement limit the Pauli exclusion (second term) can give large contributions and may not be neglected.[13]

The exciton Green function was calculated in the pole approximation

$$G(\omega,\vec{k}) = \sum_\nu \frac{|\psi_\nu\rangle\langle\psi_\nu|}{\hbar\omega - \varepsilon_\nu + i\gamma_\nu}, \quad (28)$$

where the poles $\varepsilon_\nu - i\gamma_\nu$ have been calculated in Sec. III.

We have calculated the two-photon absorption spectrum of a linear chain of large spherical semiconductor quantum dots. The signal is given by $S_{\rm TPA} \propto {\rm Im}P^{(3)}E$, with $P^{(3)}$ given by Eq. (22). We chose $\vec{k}_1 = -\vec{k}_2 = \vec{k}_3 = \vec{k}$ and $\omega_1 = -\omega_2 = \omega_3 = \omega$, and the response is proportional to ${\rm Im}P^{(3)}(\omega_s,\vec{k}_s)$. To simplify the calculation, we assumed a constant diagonal Coulomb matrix element V, with the correct asymptotic size behavior, i.e., $V \equiv v/R^3$.

We are interested in the enhancement with the size of the nonlinear response, due to cooperativity between QD's, compared with a random collection of particles. The third-order polarization has the same form as in Ref. 6. Super-radiant states are expected to play a major role and the key quantity is the ratio of oscillator strength and nonradiative decay rate which tends to redistribute this oscillator strength among several exciton states. Note that the nonradiative damping (denoted $\gamma_{\rm nr}$ hereafter) is essential for the constitency of the perturbative expansion. Indeed, if $\gamma_{\rm nr} = 0$, the expansion in increasing orders of the field is divergent at resonance since pure radiative decay rates (γ_r) of different states vanish one by one with increasing size. The linear polarization is, however, well defined since it contains the oscillator strength (f), which is proportional to the radiative decay, in the numerator. One can show that the nth-order polarization scales as $f^{(n+1)/2}/\gamma_r^n \sim 1/\gamma_r^{(n-1)/2}$. This illustrates that the connection between the nonlinear response of a nanostructure and a bulk material is not simple. Nevertheless, we assume here a constant nonradiative decay rate such that $\gamma_{\rm nr} \gg \gamma_r$. In this case, the resonant third-order polarization per unit volume scales as

$$P^{(3)} \sim \frac{\gamma_r^2}{\gamma_{\rm nr}^3}\frac{V/R^3}{\gamma_{\rm nr} - iV}. \quad (29)$$

Therefore, enhancement will be achieved when γ_r is increased and $V \gg \gamma_{\rm nr}$. The first condition is met with cooperativity (periodic assembly of QD's), whereas the second occurs for not too large QD, due to the scaling with size of the Coulomb exciton-exciton interaction. The latter does not depend on the interaction between quantum dots. A regular array will show an enhanced nonlinear polarization directly, due to the square of the radiative decay, that is $c^2/(\omega R)^2$ for spherical quantum dots. Application to CuCl gives a factor of 100 for a $10a_0$ QD array. A similar conclusion has been reached by Takagahara[11] with a simple model of a 3D-QD crystal, where the enhancement is due to the decrease of the macroscopic exciton effective mass.

In Fig. 5(b), we display the imaginary part of the third-order polarization in a two-photon absorption experiment, for a linear chain of QD's with various radii, ranging from $R = 10a_0$ to $R = 30a_0$. The lattice constant is $d = 2R$ and $\hat{\mu}_{\rm cv}$ is parallel to the axis of the chain. We chose the incoming field parallel to the chain axis, so that the $\vec{k} = 0$ exciton is created, and the nonradiative decay rate is $\gamma_{\rm nr} = 10^{-3}E_R$. Figure 5(a) gives the same calculation for a single quantum dot.

Figure 6 shows the variation with dot size of the max-

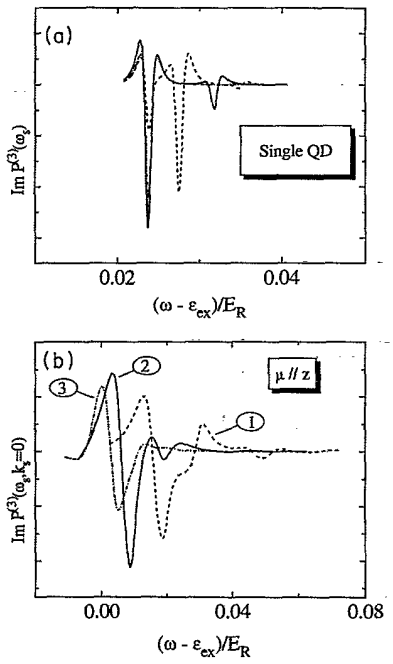

FIG. 5. (b) The imaginary part of the third-order polarization in a two-photon absorption experiment, for a linear chain of QD's with different radii curve 1: $R = 10a_0$, curve 2 $R = 20a_0$, and curve 3 $R = 30a_0$. The lattice constant is $a = 2R$ and $\hat{\mu}_{\rm cv} \parallel \hat{z} = 0$. (a) The corresponding calculation for a single quantum dot.

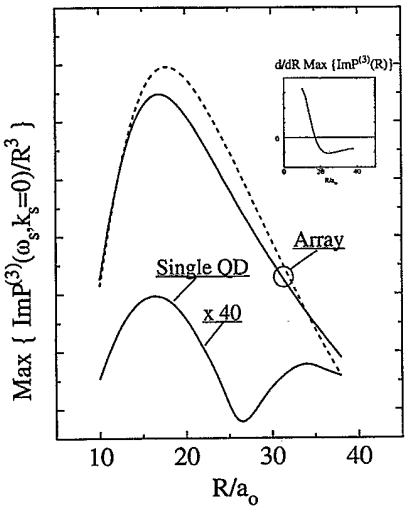

FIG. 6. Maximum amplitude of the imaginary part of the third-order polarization per unit volume shown in Fig.5. Dashed line is the result of taking only $\ell = 0$ exciton states (dipole approximation). For comparison, we give also the amplitude for a single quantum dot. The ratio between the maxima is $\simeq$ 50–100, which corresponds to cooperative enhancement.

imum value of $S_{\rm TPA}$. The dashed line was obtained by keeping only $l = 0$ exciton states. The maximum gives the optimum size for strong nonlinearities. As a reference, we give the same quantity calculated for a single quantum dot. The enhancement is two orders of magnitude compared to a single QD, and the optimal radius is around $18a_0$ for this set of parameters. This corresponds to $R \simeq 120$ Å in the case of CuCl.

VI. PHOTONIC BAND STRUCTURE OF A QUANTUM-DOT ARRAY

In this section, we show how to express the optical respone of a QD array, using the response functions of a single quantum dot. In Sec. II, we calculated the linear polarization through an equation of motion for the macroscopic exciton. The procedure given below allows us to treat also other types of materials such as metallic particles. The equations of motion in the case of plasmons (instead of excitons) involve many-body interactions, which are not easily treated self-consistently using equations of motion of one excitation.

The electric Maxwell field propagating in the array satisfies the integral equation:

$$\vec{E}(\vec{r}) = \vec{E}_0(\vec{r}) + \int d\vec{r}\,'\; \mathcal{G}(\vec{r},\vec{r}\,';\omega)\cdot\vec{P}(\vec{r}\,'), \qquad (30)$$

$$\mathcal{G}(\vec{r},\vec{r}\,';\omega) = \left\{\left(\frac{\omega}{c}\right)^2 + \vec{\nabla}\cdot\vec{\nabla}\right\}\frac{e^{i\frac{\omega}{c}|\vec{r}-\vec{r}\,'|}}{|\,\vec{r}-\vec{r}\,'\,|},$$

where $\vec{E}_0$ is the external field, and the total polarization is given formally by

$$\vec{P}(\vec{r}) = \sum_n \int_\Omega d\vec{x}\,'\; \alpha_{\rm NL}(\vec{r},\vec{x}\,',\vec{E})\vec{E}(\vec{x}\,'+\vec{R}_n), \qquad (31)$$

$\alpha_{\rm NL}(\vec{r},\vec{r}\,',\vec{E})$ is the total nonlinear polarizability of each quantum dot. It is the only quantity needed to calculate the optical response of the entire array. As before, integrals over $\vec{r}$ apply to the entire system, whereas integrals on $\vec{x}$ refer to the volume of one quantum dot only.

For nonlinear response, Eq. (30) may be calculated using numerical methods. However, if the nonlinearities are weak compared to the linear response, we can solve it perturbatively. Let the total polarization be

$$\alpha_{\rm NL}(\vec{r},\vec{r}\,',\vec{E}) = \alpha(\vec{r},\vec{r}\,') + \int d\vec{r}_1\;\beta(\vec{r},\vec{r}_1,\vec{r}\,')\vec{E}(\vec{r}_1) \qquad (32)$$
$$+ \int d\vec{r}_1 \int d\vec{r}_2\;\gamma(\vec{r},\vec{r}_1,\vec{r}_2,\vec{r}\,')\vec{E}(\vec{r}_1)\vec{E}(\vec{r}_2),$$

then, the field to first order is

$$\vec{E}^{(1)}(\omega,\vec{r}) = \int d\vec{r}\,'\Pi(\vec{r},\vec{r}\,';\omega)\vec{E}_0(\omega,\vec{r}\,'), \qquad (33)$$

where we have defined

$$\Pi(\vec{r},\vec{r}\,';\omega) \equiv \frac{1}{1-\mathcal{G}(\omega)\alpha(\omega)} \qquad (34)$$
$$= \delta(\vec{r},\vec{r}\,') + \int d\vec{r}\,''\mathcal{G}(\vec{r},\vec{r}\,'';\omega)$$
$$\times\alpha(\vec{r}\,'',\vec{r}\,';\omega) + \cdots.$$

Due to translational invariance we can use the property:

$$\vec{E}_{\vec{k}}(\vec{r}) = \vec{E}_{\vec{k}}(\vec{r}+\vec{R}_n)e^{\vec{k}\cdot\vec{R}_n}, \qquad (35)$$

where $\vec{k}$ is the Bloch wave vector. The Π operator therefore becomes local and is given by

$$\Pi(\vec{x},\vec{x}\,';\omega,\vec{k}) = \frac{1}{1-\mathcal{G}(\omega,\vec{k})\alpha(\omega)}\,, \qquad (36)$$

$$\Big[\mathcal{G}(\omega,\vec{k})\alpha(\omega)\Big](\vec{x},\vec{x}\,') = \sum_n \int_\Omega d\vec{x}\,''\mathcal{G}(\vec{x},\vec{x}\,''+\vec{R}_n;\omega)$$
$$\times e^{i\vec{k}\cdot\vec{R}_n}\alpha(\vec{x}\,'',\vec{x}\,';\omega)\,. \qquad (37)$$

The sum over the lattice sites in (37) gives the structure factor, which contains all the relevant information on the geometry of the system. In particular, the photonic band structure[3] is easily obtained from the poles of $\Pi(\omega)$, for the case of a local nonresonant polarizability $\alpha(\vec{x}-\vec{x}\,') = (\varepsilon_{\rm int}-\varepsilon_{\rm ext})\delta(\vec{x}-\vec{x}\,')$, where $\varepsilon_{\rm int}$ and $\varepsilon_{\rm ext}$ are the interior and exterior dielectric functions, respectively. If α is the excitonic polarizability, i.e.,

$$\alpha(\vec{x},\vec{x}\,') = -\sum_a \frac{\hat{\mu}_{\rm cv}\phi_a(x,x)^*\phi_a(x',x')\hat{\mu}_{\rm cv}}{\hbar\omega-\varepsilon_a^0+i0^+}, \qquad (38)$$

one recovers the results of Sec. II.

Finally, let us express the nonlinear response of the array in terms of the first-order field. Using Eq. (33), we get

$$\vec{P}^{(2)}(\omega;\vec{r}) = \int d\vec{x}_1 d\vec{x}'_1 d\vec{x}_2 d\vec{x}'_2 \; \beta(\vec{r},\vec{x}_1,\vec{x}_2;\omega,\omega_1,\omega_2)\Pi(\vec{x}_1,\vec{x}'_1;\omega_1,\vec{k}_1)\vec{E}_{0\vec{k}_1}(\omega_1,\vec{x}'_1)\Pi(\vec{x}_2,\vec{x}'_2;\omega_1,\vec{k}_1)\vec{E}_{0\vec{k}_2}(\omega_1,\vec{x}'_2) \; , \tag{39}$$

$$\begin{aligned}\vec{P}^{(3)}(\omega;\vec{r}) = \int d\vec{x}_1 d\vec{x}_2 d\vec{x}_3 d\vec{x}'_1 d\vec{x}'_2 d\vec{x}'_3 \; \gamma(\vec{r},\vec{x}_1,\vec{x}_2,\vec{x}_3;\omega,\omega_1,\omega_2,\omega_3)\Pi(\vec{x}_1,\vec{x}'_1;\omega_1,\vec{k}_1)\vec{E}_{0\vec{k}_1}(\omega,\vec{x}'_1) \\ \times\Pi(\vec{x}_2,\vec{x}'_2;\omega_2,\vec{k}_2)\vec{E}_{0\vec{k}_2}(\omega,\vec{x}'_2)\Pi(\vec{x}_2,\vec{x}'_3;\omega_3,\vec{k}_3)\vec{E}_{0\vec{k}_3}(\omega,\vec{x}'_3) \; .\end{aligned} \tag{40}$$

From these expressions it is clear that Π leads to the local field correction in the case of a small QD or a molecule.[15,16]

VII. CONCLUDING REMARKS

In this paper, we have studied the macroscopic elementary excitations of arrays of small and large semiconductor quantum dots. We assumed an infinite confining well in each QD leading to intradot and interdot exciton motion of Wannier and Frenkel types, respectively. No overlapp of electronic wave functions between QD's were considered.

Periodic assemblies of such particles have been fabricated recently[2] and many important effects such as exciton cooperativity and surface polaritons can be examined both theoretically and experimentally using artificial quantum structures. Size and shape of the QD's as well as the dimensionality or lattice constant can be controlled much more easily compared with a crystal.

In Sec. III, we have calculated the polariton modes of one-dimensional arrays of weakly confined semiconductor QD's. Our model includes the nonlocal dynamics of excitations inside each QD, as well as throughout the array. We then obtained generalized polariton modes constructed from single-QD confined polaritons,[6] which have Frenkel-exciton-polariton character.

When only single QD s-exciton states are taken into account (point-dipole approximation), the polariton dispersion relation may be expressed in a closed form, which provides a clear explanation for the existence of one super-radiant and many subradiant states. This concentration of oscillator strength in a single super-radiant state breaks down if one takes into account $\ell \neq 0$ single-QD exciton states. This illustrates the limitation of the point-dipole approximation comonly used in the Frenkel-exciton model.

Section IV was devoted to arrays made of strongly confined semiconductor QD's. We used the long wavelength approximation on each QD, but not on the scale of the lattice constant. Again we found common Frenkel-exciton-polariton character in the case of a 1D array.

The results of Sec. III were applied for the calculation of the nonlinear response of the 1D chain in a degenerate two-photon absorption experiment. We showed that nonlinearity can be enhanced by two orders of magnitude compared with a random distribution of QD's, depending on the quantum-dot size. Finally, we showed how our model can easily be used to calculate the field propagating in a periodic assembly of quantum dots by only specifying the optical response function of each quantum dot. When the QD's are characterized by a dielectric constant and a local polarization, we recover the "photonic band structure" limit. The present formalism allows us to include resonances in any part of the spectrum in the form of a nonlocal resonant polarization. Applications to metallic particles can also be made using this formalism.

ACKNOWLEDGMENTS

We wish to thank Dr. V.V. Chernyak for very interesting and useful discussions. The support of the Air Force Office of Scientific Research, the National Science Foundation, and the Center for Photoinduced Charge Transfer is gratefully acknowledged.

APPENDIX A: EFFECTIVE HAMILTONIAN FOR AN INFINITE ARRAY OF QUANTUM DOTS

Let us denote the exciton eigenfunctions of a single quantum dot by $\phi_a(\vec{r}_e,\vec{r}_h)$ with eigenvalues ε_a^0, and $\vec{\rho}_a(\vec{r}) = \hat{\mu}_{cv}\phi_a(\vec{r},\vec{r})$. The effective Hamiltonian $H_{\rm eff}$ expanded in this basis is

$$(H_{\rm eff}(\omega,\vec{k}))_{aa'} = \varepsilon_a^0\delta_{aa'} - \Sigma_{aa'}(\omega,\vec{k}), \tag{A1}$$

where

$$\begin{aligned}\Sigma_{aa'}(\omega,\vec{k}) = \int d\vec{r}\vec{\rho}_a^*(\vec{r})\cdot(q^2+\vec{\nabla}\vec{\nabla}\cdot) \\ \times\int d\vec{r}'\mathcal{G}_q(\vec{r},\vec{r}')\vec{\rho}_{a'}(\vec{r}').\end{aligned} \tag{A2}$$

Exciton states are identical on each sphere and the Bloch theorem allows us to use the following property:

$$\vec{\rho}_\lambda(\vec{x}+\vec{R}_n) = e^{i\vec{k}\cdot\vec{R}_n}\vec{\rho}_\lambda(\vec{x}), \tag{A3}$$

in (A2). Therefore,

$$\begin{aligned}\Sigma_{aa'}(\omega,\vec{k}) = i4\pi q \sum_{LM;l_1m_1;l_2m_2} J^{l_1m_1}_{LM;l_2m_2}(q,\vec{k}) \\ \times\Big[\vec{f}^{(1)*}_{al_1m_1}(q)\cdot\vec{f}^{(1)}_{a'l_2m_2}(q) \\ -f^{(2)*}_{al_1m_1}(q)f^{(2)}_{a'l_2m_2}(q)\Big] + A^0_{aa'}(\omega).\end{aligned} \tag{A4}$$

The last term is the self-interaction of a single sphere:

$$\Sigma^0_{aa'}(\omega) = \int_\Omega d\vec{x}\vec{\rho}^*_a(\vec{x})\cdot(q^2+\vec{\nabla}\vec{\nabla}\cdot) \times \int_\Omega d\vec{x}'\mathcal{G}_q(\vec{x},\vec{x}')\vec{\rho}_{a'}(\vec{x}'). \quad \text{(A5)}$$

The first term contains all the information on the geometry of the array, and J is the structure factor,

$$J^{l_1m_1}_{LM;l_2m_2}(q,\vec{k}) = 4\pi C^{l_1m_1}_{LM;l_2m_2}\left(\sum_{\vec{R}_n\neq 0} h^{(1)}_L(qR_n)Y^*_{LM}(\hat{R}_n)e^{i\vec{k}\cdot\vec{R}_n}\right), \quad \text{(A6)}$$

where $C^{l_1m_1}_{LM;l_2m_2} = i^{l_1-l_2-L}\int d\hat{r}Y^*_{l_1m_1}(\hat{r})Y_{LM}(\hat{r})Y_{l_2m_2}(\hat{r})$. When $q\to 0$, it gives the dipole-dipole interaction between two QD's. The $f^{(i)}_{al_1m_1}(q)$ are proportional to the exciton-oscillator strengths,

$$f^{(1)}_{al_1m_1}(q) = q\int d\vec{r}\vec{\rho}_a(\vec{r})j_{l_1}(qr)Y^*_{l_1m_1}(\hat{r}),$$
$$f^{(2)}_{al_1m_1}(q) = \int d\vec{r}\ \vec{\nabla}\cdot\vec{\rho}_a(\vec{r})j_{l_1}(qr)Y^*_{l_1m_1}(\hat{r}).$$

Equation (A4) is valid for quantum dot of arbirary shapes and materials. Their shape enters only in the calculation of the integrals, and the nature of material defines the dipole densities $\vec{\rho}_a(\vec{r})$.

The structure factor is calculated by the Ewald method. The general formula (valid for all dimensions) is related to the scalar Green function by the relation[10]

$$\mathcal{G}_q(\vec{R}) = -\frac{\cos(qR)}{4\pi R} + \sum_{lm} i^l\mathcal{D}_{lm}j_l(qR)Y_{lm}(\hat{R}), \quad \text{(A7)}$$

$$\mathcal{D}_{lm} = -qi^{1-l}\sum_{\vec{R}_n\neq 0} h^{(1)}_l(qR)Y^*_{lm}(\hat{R})e^{i\vec{k}\cdot\vec{R}_n} - \delta_{l0}\frac{iq}{\sqrt{4\pi}}, \quad \text{(A8)}$$

and alternatively

$$\mathcal{D}_{lm} = \lim_{R\to 0}\frac{1}{j_l(qR)}\oint d\hat{R}\ Y^*_{lm}(\hat{R})\left[\mathcal{G}_q(\vec{R}) + \frac{\cos(qR)}{4\pi R}\right] \quad \text{(A9)}$$

$$= \mathcal{D}^{(1)}_{lm} + \mathcal{D}^{(2)}_{lm} + \mathcal{D}^{(3)}_{00}\delta_{l0} \quad \text{(A10)}$$

$\mathcal{D}^{(3)}_{00}$ does not depends on the dimension and is given by[10]

$$\mathcal{D}^{(3)}_{00} = -\frac{\sqrt{\eta}}{2\pi}\sum_{n\geq 0}\frac{(q^2/\eta)^n}{n!(2n-1)}. \quad \text{(A11)}$$

One-dimension case

We choose the momentum $\vec{k}$ along the $\hat{z}$ axis. Using the cylindrical symmetry, the structure factor is not zero only for $m=0$. We find

$$\mathcal{D}^{(1)}_{l0} = -\sqrt{\frac{2l+1}{8\pi^3a^2}}\left(\frac{i}{q}\right)^l\sum_{k_n}\sum_{p=0}^{E(l/2)}\frac{(1)^p(2p)!}{4^p p!} \times(k_n+k)^{l-2p}\int_{1/\eta}^\infty\frac{e^{bt}}{t^{p+1}}, \quad \text{(A12)}$$

$$\mathcal{D}^{(2)}_{l0} = -\frac{\sqrt{2l+1}}{8\pi^2}\frac{1}{(2q)^l}\sum_{R_n\neq 0}e^{ikR_n} \times R_n^l\int_\eta^\infty dt\ t^{l-1/2}e^{q^2/t-R_n^2t/4}, \quad \text{(A13)}$$

where $b = q^2-(k_n+k)^2$, a is the lattice parameter, and η an arbitrary chosen convergence factor, which can choose real and positive. The above integrals should be undestood as contour integrals. In particular,

$$\int_{1/\eta}^{e^{i\varphi}\infty}\frac{e^{bt}}{t^{p+1}} = b^p\,\Gamma(-p,b/\eta) \quad \text{(A14)}$$

is the incomplete γ function of complexe argument. When $b<0$ the integral is purely real, but if $b>0$ one must integrate over a complex path to avoid the pole in $t=0$, for in this case $\varphi=-\pi$. This reflects the radiative to nonradiative change of the exciton as b changes.

APPENDIX B: EXACT EXCITON DISPERSION RELATION FOR AN ARRAY OF WEAKLY CONFINED *S* EXCITONS

If we restrict the QD eigenstates to symetric (s) states, then the matrix Σ becomes much simpler and is given by

$$\Sigma_{\lambda\lambda'}(q,\vec{k}) = \delta_{ll'0}\Sigma_{nn'}(q,\vec{k}) \quad \text{(B1)}$$
$$= \delta_{ll'0}\left[\Sigma^0_{nn'}(q,\vec{k}) + \delta_{nn'}g_n(q)\right], \quad \text{(B2)}$$

where

$$\Sigma^0_{nn'} = C(q,\vec{k})f_n(q)f_{n'}(q). \quad \text{(B3)}$$

The above functions are given in Appendix A. The quantity $C(q,\vec{k})$, defined by this equation, contains all the information on the lattice (structure factor) and depends on the functions J defined by (A6). The eigenvalues are determined by the following equation:

$$1 = -C(q,\vec{k})\sum_n\frac{f_n(q)^2}{\hbar\omega-\varepsilon^0_n+g_n(q)} \quad \text{(B4)}$$

$$= \frac{C(q,\vec{k})}{4\pi\delta}\sum_{i=1,2,3}k_i\frac{\cot g[\frac{\pi}{2}(k_i-1)]}{\prod_{j\neq i}(k_j^2-k_i^2)}, \quad \text{(B5)}$$

and k_i are polariton wave vectors in each QD.

The eigenvectors are given by

$$|\psi_\nu\rangle = \sum_n\frac{f_n}{[\varepsilon_\nu-\varepsilon^0_n+g_n(q)]}|u_n\rangle, \quad \text{(B6)}$$

where $|u_n\rangle$ are the eigenvectors of the bare Hamiltonian H_0 and ε_ν the solutions of Eq. (B4). These simple forms of the eigenvalue equation and eigenvectors are a *conse-*

quence of the form of the matrix Σ, and their validity can be verified directly by substitution.

We next consider an interesting limiting case. Ignoring retardation and focusing only on the dipole-dipole interaction, we obtain the following Hamiltonian:

$$H_{nn'}(\vec{k}) = \left(\varepsilon_n^0 + \frac{\Delta_{\rm LT}}{3}\right)\delta_{nn'} + \frac{2}{\pi^2}\frac{\Delta_{\rm LT}}{nn'}\mathcal{L}(\vec{k}), \qquad \text{(B7)}$$

where $\Delta_{\rm LT}$ is the exciton longitudinal-transverse splitting in the bulk.

$$\mathcal{L}(\vec{k}) = \sum_{\vec{R}_p \neq \vec{0}} \frac{(1-3\cos^2\theta)}{R_p^3} e^{i\vec{k}\cdot\vec{R}_p}, \qquad \text{(B8)}$$

and the eigenvalues ω are obtained from the equation

$$1 = -\frac{\Delta_{\rm LT}}{\delta\pi}\mathcal{L}(\vec{k})\left\{\frac{1}{\pi z^2}\left(\frac{\pi^2}{3} - \frac{1}{z^2}\right) + \frac{1}{z^3}\cot g(\pi z)\right\}, \qquad \text{(B9)}$$

with $z^2 = (\hbar\omega - \varepsilon_{\rm exc} - \frac{\Delta_{\rm LT}}{3})/\delta$, $\delta = \hbar^2/2MR^2$. This is a generalization of the Frenkel-exciton result when each molecule is characterized by an infinite number of s states and particle-in-a-box wave functions. The eigenvectors are easily obtained from Eq. (B6). The right-hand side of Eq. (B9) without the structure factor $\mathcal{L}(\vec{k})$ is actually the polarizability of a QD in the long wavelength approximation. When the QD's are not too large (i.e., the band width is small compared to $\varepsilon_n^0 - \varepsilon_{n'}^0$), the exciton energy spectrum is simply

$$E_n(\vec{k}) = \varepsilon_n^0 + \frac{\Delta_{\rm LT}}{3} + \frac{2}{\pi^2}\frac{\Delta_{\rm LT}}{n^2}\mathcal{L}(\vec{k}). \qquad \text{(B10)}$$

In the same approximation, we see that the radiative decay is

$$\gamma_n^0 = \frac{4}{3}\frac{(qR)^3\Delta_{\rm LT}}{n^2\pi^2} \qquad \text{(B11)}$$

for one QD and becomes

$$\gamma_n(\vec{k}) = \gamma_n^0\left(1 + {\rm Re}\left\{S_0(\vec{k}) + \sqrt{\frac{1}{5}}S_2(\vec{k})\right\}\Big/\sqrt{4\pi}\right) \qquad \text{(B12)}$$

for an infinite array. Note that this last expression vanishes for $q \leq k$.

$$S_l(\vec{k}) = 4\pi\sum_{\vec{R}_p\neq\vec{0}} h_l^{(1)}(qR_p)Y_{l0}^*(\hat{R}_p)\ e^{i\vec{k}\cdot\vec{R}_p}. \qquad \text{(B13)}$$

The structure factor is responsible for the super-radiative effect in array of QD's. The same results can be obtained directly by Fourier transform of Eq. (A4); however, we clearly demonstrate here how our model gives well-known limits. Our procedure includes all Umklapp contributions since the structure factor is summed over the entire space.

APPENDIX C: EFFECTIVE HAMILTONIAN FOR STRONG CONFINEMENT

In this appendix, we calculate the effective Hamiltonian (11) in the strong confinement limit with the wave function (18) and assuming the long wavelength approximation for a single QD.

The exciton wave function in the quantum dot (taken at the point $\vec{r}_e = \vec{r}_h = \vec{r}$ for the calculation of the self-energy Σ) is

$$\phi(\vec{r},\vec{r}) = \frac{\pi}{2R^3}j_0^2(\pi x), \qquad x = r/R. \qquad \text{(C1)}$$

The matrix Σ, i.e., the retarded interaction with the field, is then

$$\Sigma(\omega,\vec{k}) = i\frac{\Delta_{\rm LT}}{(R/a_0)^3}\left(\frac{q^3}{4}J_{00;00}^{00}(q,\vec{k}) - 4\pi \times \sum_{L=0,2;ij} J_{Lj-i;1-j}^{1-i}(q,\vec{k})\tilde{\mu}_i\tilde{\mu}_j f^{(1)}\right) + \Sigma^0(\omega). \qquad \text{(C2)}$$

The last term is the self-interaction on one sphere:

$$\Sigma^0(\omega) = \frac{\Delta_{\rm LT}}{(R/a_0)^3}\lim_{q\to 0}\left(iq^3\mu_{\rm cv}^2\int_0^1 dx\sin(\pi x)^2 h_0(qx_>) \times \int_0^1 dx' j_0(qx_<)\sin(\pi x')^2 - \frac{\pi^2}{16}\int d\vec{x}\hat{\mu}_{\rm cv}\cdot\vec{\nabla}(j_0(\pi x)^2) \times \int d\vec{x}'\frac{e^{iq|\vec{x}-\vec{x}'|}}{|\vec{x}-\vec{x}'|}\hat{\mu}_{\rm cv}\cdot\vec{\nabla}(j_0(\pi x')^2)\right). \qquad \text{(C3)}$$

In this expression, we only keep the lowest orders in q, in both the real and imaginary parts. We have also defined

$$f^{(1)} = \pi^2\lim_{q\to 0} q\left[\int_0^1 dx x^2 j_0(\pi x)j_1(\pi x) \times j_1(qx)\vec{\nabla}\left(\frac{\sin(\pi x)^2}{x^2}\right)\right]^2.$$

[1] L. Bányai and S.W. Koch, *Semiconductor Quantum Dots* (World Scientific, Singapore, 1993).

[2] V.L. Alivisatos, M.C. Schiamp, and P. Alivisatos, Nature **370**, 354 (1994).

[3] E. Yablonovich and T.J. Gmitter, Phys. Rev. Lett. **63**, 1950 (1989).

[4] S. John and R. Rangarajan, Phys. Rev. B, **38**, 10181 (1988).

[5] Y. Ohfuti and K. Cho, in *Proceedings of the International Symposium on Foundations of Quantum Mechanics '92,*

Hatoyama, Japan, edited by H. Ezawa and Y. Murayama (North-Holland, Amsterdam, 1993).
[6] L. Belleguie and S. Mukamel, J. Chem. Phys. **101**, 9719 (1994).
[7] A.S. Davydov, *Theory of Molecular Exciton* (Plenum, New York, 1971).
[8] M. Orrit, C. Aslangul, and P. Kottis, Phys. Rev. B **25**, 7263 (1982).
[9] V. Chernyark and S. Mukamel, Phys. Rev. B, **48**, 2470 (1993).
[10] F.S. Ham and B. Segall, Phys. Rev. **124**, 1786 (1961).
[11] T. Takagahara, *Nonlinear Optics*, edited by S. Miyata (Elsevier, New York, 1992), p. 85.
[12] L. Belleguie and L. Bányai, Phys. Rev. B **44**, 8785 (1991).
[13] D.S. Chemla, J.-Y. Bigot, M.-A. Mycek, S. Weiss, and W. Schäfer, Phys. Rev. B **50**, 8439 (1994).
[14] H. Haug and S.W. Koch, *Quantum Theory of the Optical and Electronic Properties of Semiconductors* (World Scientific, Singapore, 1990).
[15] D.S. Chemla and J. Zyss, *Nonlinear Optical Properties of Organic Molecules and Crystals* (Academic Press, New York, 1986).
[16] K. Kambe, Z. Naturforsch. **22**, 322 (1967).